Letter

Phase transition during inflation and the gravitational wave signal at pulsar timing arrays

Haipeng An,[1,2,3,4,*] Boye Su,[1,†] Hanwen Tai,[5,6,‡] Lian-Tao Wang,[5,6,7,§] and Chen Yang[1,‖]

[1]*Department of Physics, Tsinghua University, Beijing 100084, China*
[2]*Center for High Energy Physics, Tsinghua University, Beijing 100084, China*
[3]*Center for High Energy Physics, Peking University, Beijing 100871, China*
[4]*Frontier Science Center for Quantum Information, Beijing 100084, China*
[5]*Department of Physics, The University of Chicago, Chicago, Illinois 60637, USA*
[6]*Enrico Fermi Institute, University of Chicago, Chicago, Illinois 60637, USA*
[7]*Kavli Institute for Cosmological Physics, University of Chicago, Chicago, Illinois 60637, USA*

(Received 25 August 2023; accepted 13 May 2024; published 18 June 2024)

The gravitational wave (GW) signal offers a promising window into the dynamics of the early Universe. The recent results from the pulsar timing arrays (PTAs) could be the first glimpse of such new physics. In particular, they could point to new details during inflation, which cannot be probed by other means. We explore the possibility that the new results could come from the secondary GWs sourced by curvature perturbations, generated by a first-order phase transition during inflation. Based on the results of a field-theoretic lattice simulation of the phase transition process, we show that the GW signal generated through this mechanism can account for the new results from the PTAs. We analyze the spectral shape of the signal in detail. Future observations can use such information to distinguish the GW signal considered here from other possible sources.

DOI: 10.1103/PhysRevD.109.L121304

Introduction. Despite the enormous progress in our knowledge of the early Universe, large gaps remain. The gravitational wave (GW) signal offers a new window into the early Universe epochs and dynamics that cannot be probed by other means. Pulsar timing array (PTA) collaborations have recently released further evidence that the previously observed common-spectrum process exhibits the Hellings-Downs angular correlation [1–7]. This finding indicates the existence of a gravitational wave background in the nanohertz frequency range [8].

The GW signal in this frequency range can emerge from various phenomena, including low-scale phase transitions in the radiation domination (RD) era [9–27], supermassive black hole binaries (SMBHBs) [28–36], and topological defects like cosmic strings and domain walls [23,37–52]. Simultaneously, this signal can also originate during inflation, approximately 15 e-folds after the cosmic microwave background modes exit the horizon. Numerous mechanisms have been investigated in relation to this possibility [53–76]. Additionally, alternative new physics scenarios have been proposed as potential sources for the observed signal [77–82]. In this work, we focus on the possibility of the source being a first-order phase transition during inflation [83–86]. The process of bubble collision during the phase transition can generate GWs, referred to as the primary GW signal, which is suppressed by $(H_{\rm inf}/\beta)^5$ and $(L/\rho_{\rm inf})^2$, with $H_{\rm inf}$ representing the Hubble expansion rate, β denoting the phase transition rate, L representing the latent heat density, and $\rho_{\rm inf}$ being the total energy density of the Universe during inflation. Meanwhile, the phase transition process serves as a source of curvature perturbations, that, after inflation, give rise to the so-called secondary GWs [87] (also see [88,89]). Compared to the primary GWs, the secondary GWs can undergo natural enhancement via the slow-roll parameter, thus potentially accounting for the signals observed by the PTAs.

As pointed out in [84,85], the plasma energy density during inflation is significantly smaller compared to latent heat. Therefore, the dominant source for GW and the induced curvature perturbation is from bubble collisions. In this work, we employ a field-theoretic simulation of the bubble nucleation and collision process to calculate the induced curvature perturbation. Based on the results, we predict both the strength and the spectral shape of the secondary GW signal. Without combining the datasets from different PTAs, we choose the results from the NANOGrav Collaboration [1] as a benchmark for comparison. We show that both the size and the shape of the

*anhp@mail.tsinghua.edu.cn
†sby20@mails.tsinghua.edu.cn
‡hanwentai@uchicago.edu
§liantaow@uchicago.edu
‖yangc18@mails.tsinghua.edu.cn

signal observed by NANOGrav [1,5] in the region with the frequency $f < (1\ \mathrm{yr})^{-1}$ can be well fit by the secondary GWs generated through first-order phase transition occurring during inflation.

The model. In this work, we model a spectator sector with a single real scalar field σ. The Lagrangian of the inflaton ϕ and the spectator σ is

$$\mathcal{L} = -\frac{1}{2} g^{\mu\nu}\partial_\mu\phi\partial_\nu\phi - \frac{1}{2} g^{\mu\nu}\partial_\mu\sigma\partial_\nu\sigma - V(\phi,\sigma). \quad (1)$$

For the convenience of later discussions, we decompose $V(\phi,\sigma)$ as

$$V(\phi,\sigma) = V_0(\phi) + V_1(\phi,\sigma), \quad (2)$$

where $V_0(\phi) = V(\phi,0)$.

We decompose ϕ into its homogeneous part ϕ_0 and the perturbation $\delta\phi$ during inflation. The excursion of ϕ_0 during inflation can be around the Planck scale. The crucial part in the Lagrangian (1) is that the mass of σ depends on ϕ_0, given by

$$m_\sigma^2 = c_m\phi_0^2 - m^2. \quad (3)$$

Consequently, the evolution of ϕ_0 affects the shape of the potential and triggers a first-order phase transition. The general framework for this scenario is discussed in [84,85]. Further details of the specific model utilized in our numerical simulation are presented in Supplemental Material [90]. The timescale of the phase transition is determined by $\beta = -dS_4/dt$, where S_4 is the bounce action between the false and true vacuums and t is the physical time.

For the class of models considered here, $\beta/H_{\mathrm{inf}} \sim \mathcal{O}(10)$ [84,85].

Through this work, we adopt the Newtonian gauge. The metric components can be written as

$$g_{00} = -a^2(1+2\Phi), \qquad g_{0i} = 0,$$
$$g_{ij} = a^2\left[\delta_{ij}(1-2\Psi) + h_{ij}\right]. \quad (4)$$

During inflation, we have $a = -1/H_{\mathrm{inf}}\tau$ with τ the conformal time. During RD, we have $a = a_R^2 H_R\tau$, where a_R and H_R are the scale factor and the Hubble parameter at reheating, respectively. In this work, we assume de Sitter inflation with instantaneous reheating, which implies $H_R = H_{\mathrm{inf}}$.

Primary and secondary GWs. In our setup, GWs can be copiously generated during and after inflation. In both cases, the GWs satisfy the differential equation

$$h_{ij}^{\mathrm{TT}\prime\prime} + 2\mathcal{H}h_{ij}^{\mathrm{TT}\prime} - \nabla^2 h_{ij}^{\mathrm{TT}} = 16\pi G\mathcal{T}_{ij}, \quad (5)$$

where "TT" denotes the transverse and traceless components, $\mathcal{H} = a'/a$, and $\mathcal{T}_{ij}$ represents the source of GWs.

During inflation, the main contribution to the GWs is from the TT components of the energy-momentum tensor composed of σ and $\delta\phi$, where $\delta\phi$ is induced by the backreaction from the phase transition as discussed later. We call these contributions primary GWs. After being produced, the primary GWs will exit the horizon, and their field strength will be frozen to fixed values. The primary GWs will oscillate again once they reenter the horizon.

In addition to the primary GWs, the phase transition also induces curvature perturbations leading to secondary GWs after inflation. In the Newtonian gauge described by Eq. (4), the source $\mathcal{T}_{ij}$ consists of terms quadratic in Φ [87,88].

The induced curvature perturbations. From the Lagrangian (1), we can derive the equation of motion for $\delta\tilde{\phi}$ (the Fourier transformation of $\delta\phi$):

$$\delta\tilde{\phi}_{\mathbf{q}}'' - \frac{2}{\tau}\delta\tilde{\phi}_{\mathbf{q}}' + \left(q^2 + \frac{1}{H_{\mathrm{inf}}^2\tau^2}\frac{\partial^2 V_0}{\partial\phi_0^2}\right)\delta\tilde{\phi}_{\mathbf{q}} = \mathcal{S}_{\mathbf{q}}, \quad (6)$$

where the source $\mathcal{S}_{\mathbf{q}}$ is

$$\mathcal{S}_{\mathbf{q}} = -\frac{1}{H_{\mathrm{inf}}^2\tau^2}\left[\frac{\partial V_1}{\partial\phi}\right]_{\mathbf{q}} - \left\{\frac{2\tilde{\Phi}_{\mathbf{q}}}{H_{\mathrm{inf}}^2\tau^2}\left(\frac{\partial V_0}{\partial\phi_0} + \left[\frac{\partial V_1}{\partial\phi}\right]_0\right) + \frac{\dot{\phi}_0}{H_{\mathrm{inf}}\tau}\left(3\tilde{\Psi}_{\mathbf{q}}' + \tilde{\Phi}_{\mathbf{q}}'\right)\right\}. \quad (7)$$

Here, the symbol $[\cdots]_{\mathbf{q}}$ denotes the Fourier mode with comoving momentum $\mathbf{q}$, and $\dot{\phi}_0$ denotes $d\phi_0/dt$. There are two source terms on the right-hand side of Eq. (6), in which the first is from the direct interaction between ϕ and σ, whereas the second is purely gravitational. In the case of a polynomial interaction $c_m\phi^2\sigma^2$, we have

$$\left[\frac{\partial V_1}{\partial\phi}\right]_{\mathbf{q}} = c_m[\phi\sigma^2]_{\mathbf{q}} \approx c_m\phi_0[\sigma^2]_{\mathbf{q}}. \quad (8)$$

According to the Einstein equations, Φ and Ψ satisfy the following differential equation:

$$\tilde{\Psi}_{\mathbf{q}}' - \frac{\tilde{\Phi}_{\mathbf{q}}}{\tau} = -4\pi G_N\left(\frac{\dot{\phi}_0\delta\tilde{\phi}_{\mathbf{q}}}{H_{\mathrm{inf}}\tau} + \left[\frac{\partial_i}{\partial^2}(\sigma'\partial_i\sigma)\right]_{\mathbf{q}}\right). \quad (9)$$

From energy-momentum conservation, we have

$$\tilde{\Phi}_{\mathbf{q}} - \tilde{\Psi}_{\mathbf{q}} = -8\pi G_N\tilde{\pi}_{\mathbf{q}}^S/(H_{\mathrm{inf}}^2\tau^2), \quad (10)$$

where π^S represents the anisotropic inertia

$$\tilde{\pi}^S_{\mathbf{q}} = -\frac{3}{2} H^2_{\rm inf} \tau^2 q_i q_j q^{-4} [(\partial_i \sigma \partial_j \sigma)^{\rm TL}]_{\mathbf{q}}, \tag{11}$$

where the superscript TL refers to the traceless part.

After the phase transition, the Universe returns to single-field inflation. Thus, the gauge-invariant quantity

$$\zeta_{\mathbf{q}} = -\tilde{\Psi}_{\mathbf{q}} - \frac{H_{\rm inf} \delta\tilde{\phi}_{\mathbf{q}}}{\dot{\phi}_0} \tag{12}$$

is conserved when evolving outside the horizon.

Power spectrum of ζ. In this work, we use a $1000 \times 1000 \times 1000$ lattice to simulate the phase transition process in de Sitter space and numerically solve Eqs. (6), (9), and (10) to calculate the various contributions to $\zeta_{\mathbf{q}}$. As discussed in the appendix of [84], the typical values for $\beta/H_{\rm inf}$ is $\mathcal{O}(10)$. The solid curves in Fig. 1 represent the numerical results of Δ^2_ζ, the spectrum of the induced curvature perturbation for $\beta/H_{\rm inf} = 4$, 5, 10, and 20. Δ^2_ζ is defined as

$$\Delta^2_\zeta(q) = \frac{q^3}{2\pi^2} P_\zeta(q) = \frac{q^3}{2\pi^2} \langle \zeta_{\mathbf{q}} \zeta^*_{\mathbf{q}'} \rangle', \tag{13}$$

where $\langle \cdots \rangle'$ denotes the correlation function without the delta function. Figure 1 shows that Δ^2_ζ grows as q^3 in the IR region (to the left of the peak) and drops as q^{-6} in the UV region (far to the right). By comparing the peak values of the curves for different $\beta/H_{\rm inf}$ in Fig. 1, it can be concluded that $\Delta^2_\zeta \propto (H_{\rm inf}/\beta)^3$.

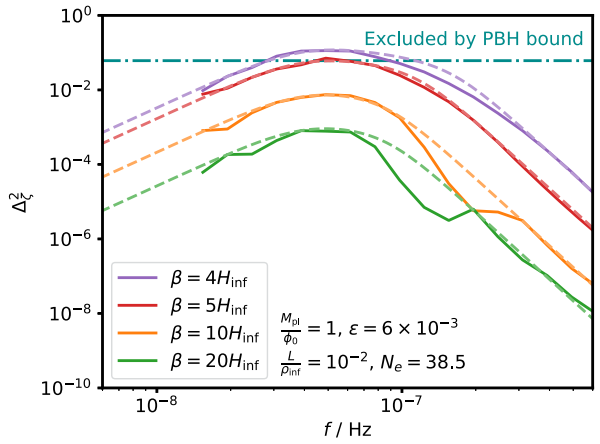

FIG. 1. Power spectrum of the induced curvature perturbation Δ^2_ζ for different choices of parameters. The solid curves are the results from numerical simulation, and the dashed curves are based on the empirical formula Eq. (20). The wiggles in the curves for $\beta/H_{\rm inf} = 10$ and 20 are the remnants of the oscillatory pattern in the integrand of (14), which also leads to the oscillatory pattern in the primary GW spectrum as discussed in [84,85]. Large curvature perturbations can result in primordial black hole (PBH) production, and the relevant constraint is indicated by the dash-dotted line [91].

To provide further insights, an approximate formula for Δ^2_ζ will be derived. Several e-folds after the phase transition, the Φ contribution to ζ becomes negligible as its direct source from σ quickly redshifts away.

Hence, using the Green's function method and Eq. (6), we obtain

$$\zeta_{\mathbf{q}} = -\frac{H_{\rm inf}}{\dot{\phi}_0 q^2} \int_{-\infty}^{0} \frac{d\tau'}{\tau'} \left(\cos q\tau' - \frac{\sin q\tau'}{q\tau'} \right) \mathcal{S}_{\mathbf{q}}(\tau'). \tag{14}$$

As discussed in Supplemental Material [90], in the parameter space of interest, the gravitational-induced contribution to the curvature perturbation is smaller than the direct contribution. Thus, in the qualitative analysis, we focus on the contribution from the direct source (the first term in $\mathcal{S}_{\mathbf{q}}$).

According to Eqs. (8) and (14), Δ^2_ζ is inversely proportional to $\epsilon \equiv \dot{\phi}_0^2/(2H^2_{\rm inf} M^2_{\rm pl})$, the slow-roll parameter after the phase transition. Assuming that the rolling of the scalar fields is predominantly in the direction of ϕ_0 after the phase transition, $\zeta_{\mathbf{q}}$ can be estimated as

$$\zeta_{\mathbf{q}} \approx \frac{H_{\rm inf}}{\dot{\phi}_0 q^2} \int \frac{d\tau'}{\tau'} \left(\cos q\tau' - \frac{\sin q\tau'}{q\tau'} \right) \frac{c_m \phi_0 [\sigma^2(\tau')]_{\mathbf{q}}}{H^2_{\rm inf} \tau'^2}. \tag{15}$$

For a first-order phase transition to complete, we require its duration $\sim \beta^{-1} < H^{-1}_{\rm inf}$. However, even after the phase transition, the σ field continues to oscillate and produce ζ. Since $\beta < m_\sigma$, these oscillations resemble matterlike behavior and redshift as a^{-3}. Thus, the ζ production diminishes within a few e-folds after the phase transition. Figure S2 in Supplemental Material [90] shows that majority of induced curvature perturbations occur between one and two e-folds after the phase transition begins.

For modes with $q_{\rm phys} < H_{\rm inf}$, or, equivalently, $q\tau' < 1$, a Taylor expansion of the cosine and sine functions in the integrand of Eq. (15) can be performed, resulting in

$$\zeta_{\mathbf{q}} \approx \frac{1}{3\dot{\phi}_0} \int dt' c_m \phi_0 [\sigma^2(\tau')]_{\mathbf{q}}, \tag{16}$$

where $dt' = a(\tau')d\tau'$. Considering that the typical scale of the bubble size is β^{-1} and $H_{\rm inf} < \beta$, the correlation $\langle [\sigma^2]_{\mathbf{q}} [\sigma^2]_{\mathbf{q}'} \rangle'$ is expected to be insensitive to $\mathbf{q}$. Since the term $c_m \phi_0^2 \sigma^2$ triggers the phase transition, we also expect $c_m \phi_0^2 \sigma^2 \sim L$. Hence, we have

$$\int dt' \int dt'' c_m^2 \phi_0^2 \langle [\sigma^2(\tau')]_{\mathbf{q}} [\sigma^2(\tau'')]_{\mathbf{q}'} \rangle' \sim \frac{L^2}{H^2_{\rm inf} a^6_\star} \left(\frac{2\pi}{\beta} \right)^3, \tag{17}$$

where $a_\star$ is the scale factor at the time of the phase transition. The factor $H^{-2}_{\rm inf}$ arises due to the integration over the physical time duration, and the factor $(2\pi/\beta)^3$ is from

dimensional analysis. The factor $a_\star^6$ appears in the denominator because the Fourier transformation is performed in comoving space. Combining Eqs. (16) and (17), in the region $q_{\rm phys} < H_{\rm inf}$, we have

$$\Delta_\zeta^{2(\rm IR)}(q) = A_{\rm ref}\left(\frac{q_{\rm phys}}{H_{\rm inf}}\right)^3, \tag{18}$$

where

$$A_{\rm ref} = \frac{\mathcal{A}}{\epsilon}\left(\frac{M_{\rm pl}}{\phi_0}\right)^2\left(\frac{H_{\rm inf}}{\beta}\right)^3\left(\frac{L}{\rho_{\rm inf}}\right)^2. \tag{19}$$

The numerical factor $\mathcal{A}$ is determined by the specific phase transition model. Numerical simulations show that $\mathcal{A} \approx 24$ for the model used in this work. Equation (18) explains the IR behavior, the $(H_{\rm inf}/\beta)^3$ dependence, and the $(L/\rho_{\rm inf})^2$ dependence of Δ_ζ^2 depicted in Fig. 1.

The q^3 growth of Δ_ζ^2 stops when $q_{\rm phys}$ reaches H. In the region where $q_{\rm phys} \gtrsim H_{\rm inf}$, the sine and cosine terms in (15) are of the order of one, while $\langle [\sigma^2]_{\mathbf{q}}[\sigma^2]^*_{\mathbf{q}'}\rangle'$ remains insensitive to changes of q. By counting the power of q, it can be concluded that Δ_ζ^2 drops as q^{-1} in this region.

As shown in Supplemental Material [90], the production of the curvature perturbation lasts for a few e-folds, during which the typical physical momentum of the bubbles undergoes redshifting. As a result, the correlation $\langle [\sigma^2]_{\mathbf{q}}[\sigma^2]^*_{\mathbf{q}'}\rangle'$ drops significantly as $q_{\rm phys}$ become larger than a value between H and β. This behavior leads to the drop of Δ_ζ^2 as q^{-6} in the UV region, as shown in Fig. 1.

In summary, we arrive at an empirical formula for Δ_ζ^2:

$$\Delta_\zeta^{2(\rm emp)}(q) = A_{\rm ref}\mathcal{F}\left(\frac{q_{\rm phys}}{H_{\rm inf}}\right), \tag{20}$$

where

$$\mathcal{F}(x) = \frac{x^3}{1 + (\alpha_1 x)^4 + (\alpha_2 x)^9}. \tag{21}$$

Numerical results give that $\alpha_1 = 0.31$, while α_2 mildly depends on $\beta/H_{\rm inf}$ and equals 0.143, 0.17, 0.2, and 0.2 for $\beta/H_{\rm inf} = 4$, 5, 10, and 20, respectively.

In a general inflation model, ϕ_0 and ϵ can be independent parameters. For single-field inflation, if we consider the case that $\partial V_1/\partial\phi$ dominates the evolution of ϕ_0 after the phase transition, we have

$$\epsilon = \frac{\dot\phi_0^2}{2M_{\rm pl}^2 H_{\rm inf}^2} \sim \frac{(V_1')^2}{6\rho_{\rm inf}H_{\rm inf}^2}, \tag{22}$$

and, assuming V_1 is a polynomial in ϕ,

$$\frac{M_{\rm pl}^2}{\phi_0^2} \sim \left(\frac{M_{\rm pl}}{V_1/V_1'}\right)^2 \sim \left(\frac{M_{\rm pl}}{L/V_1'}\right)^2. \tag{23}$$

Thus, without fine-tuning, the peak value of Δ_ζ^2 is

$$\Delta_\zeta^2(q) \approx 3.6 \times \left(\frac{H_{\rm inf}}{\beta}\right)^3 \mathcal{F}\left(\frac{q_{\rm phys}}{H_{\rm inf}}\right), \tag{24}$$

suggesting that, for $H_{\rm inf}/\beta \sim 0.1$, a peak value of Δ_ζ^2 around 0.01 can be naturally expected.

Production of secondary GWs. To produce the GWs to account for the PTA results, the curvature perturbations need to reenter the horizon well before the matter-radiation equality.

Following the procedure outlined in [88], the spectrum function for the secondary GWs can be derived as

$$\Omega_{\rm GW}^{(2)}(f) = \Omega_R A_{\rm ref}^2 \mathcal{F}_2\left(\frac{q_{\rm phys}}{H_{\rm inf}}\right), \tag{25}$$

where Ω_R is the radiation energy density of the Universe. The form factor $\mathcal{F}_2$ collects transfer functions and Green's functions. As shown in Supplemental Material [90], $\mathcal{F}_2(x)$ peaks around $x = 5$, and its peak value is about 200. In the IR region, we have

$$\mathcal{F}_2^{\rm IR}(x) \approx x^3\left(\frac{6}{5}\log^2 x + \frac{16}{25}\log x + \frac{28}{125}\right). \tag{26}$$

The logarithmic structure in $\mathcal{F}_2$ slows down the rise of the spectrum, allowing for a better fit to the IR part of the NANOGrav observation data as depicted in Fig. 2.

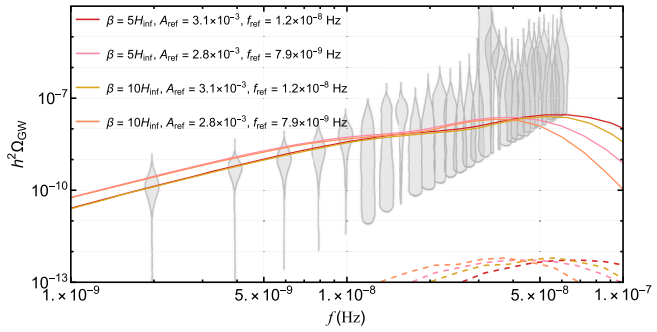

FIG. 2. The differential spectra of secondary GWs induced by first-order phase transitions during inflation for different parameters as shown in the plot. The gray violins show the periodogram for an Hellings-Downs-correlated free spectral process from [92]. Four sets of the model parameters are shown as examples, which match the data collected by the NANOGrav Collaboration in terms of the amplitude and spectral shape, particularly in the region $f < 3 \times 10^{-8}$ Hz. The corresponding primary GW spectra are represented by the dashed curves. In the parameter region of interest, the magnitude of the primary GWs is smaller than the secondary GWs by a few orders of magnitude.

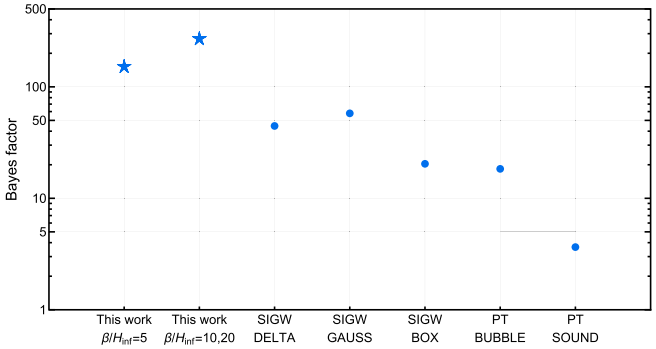

FIG. 3. The Bayes factors for the model comparisons between the new physics interpretations of the signal and the interpretation based solely on SMBHBs. The stars denote the Bayes factors for the model considered in this work. Other results labeled as "SIGW DELTA," "SIGW GAUSS," "SIGW BOX," "PT BUBBLE," and "PT SOUND" are the benchmark new physics models studied in [92]. SIGW and PT stand for scalar-induced GWs and phase transition, respectively.

The relation between the comoving momentum q and today's frequency f is

$$f = \frac{q}{2\pi a_0} = f_{\rm ref} \times \frac{q_{\rm phys}}{H_{\rm inf}}, \tag{27}$$

where

$$f_{\rm ref} = 10^{-9}\ {\rm Hz} \times e^{40-N_e} \left(\frac{H_{\rm inf}}{10^{14}\ {\rm GeV}}\right)^{1/2}. \tag{28}$$

N_e is the number of e-folds the phase transition happened before the end of inflation. Here, we assume the reheating process finished within one e-fold. Thus, if the phase transition is responsible for the PTA signals, it happened about 40 e-folds before the end of inflation.

Utilizing the Bayesian analysis developed by the NANOGrav Collaboration [93] (also described in Supplemental Material [90]), we present the Bayes factor for the model comparisons between our work and the interpretation in terms of SMBHBs in Fig. 3 accompanied with the benchmark model chosen by the NANOGrav group [92], where we can see that the Bayes factor of our model is significantly higher than the benchmark models in [92]. Figures 4 and 5 display the reconstructed posterior distributions of our scenario, indicating that the benchmarks presented in Fig. 2 fall within the 1σ contour. It is interesting to note that the scenario for $\beta/H_{\rm inf} = 20$ is exactly the same as that for $\beta/H_{\rm inf} = 10$ in Figs. 3 and 5, due to the fact that they share both form factors $\mathcal{F}(\frac{q_{\rm phys}}{H_{\rm inf}})$ and $\mathcal{F}_2(\frac{q_{\rm phys}}{H_{\rm inf}})$. Therefore, the spectra of secondary GWs for $\beta/H_{\rm inf} = 20$ completely overlap with those for $\beta/H_{\rm inf} = 10$ but with different primary GWs.

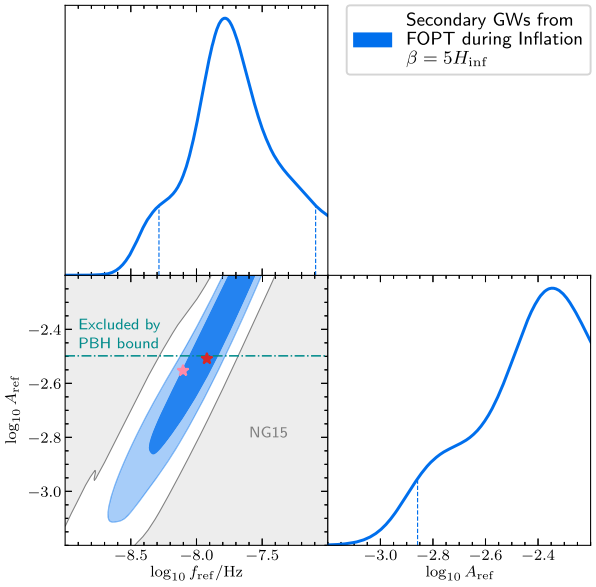

FIG. 4. The reconstructed posterior distributions for the parameters, $A_{\rm ref}$ and $f_{\rm ref}$ for $\beta = 5H_{\rm inf}$. The upper left and lower right panels display the 1D marginalized distributions with the 68% Bayesian credible intervals, while the lower left panel depicts the 68% (darker) and the 95% (lighter) Bayesian credible regions in the 2D posterior distribution. The two benchmark stars correspond to the two curves with the same color shown in Fig. 2. The PBH bound on the curvature perturbation is also shown by the dash-dotted curve.

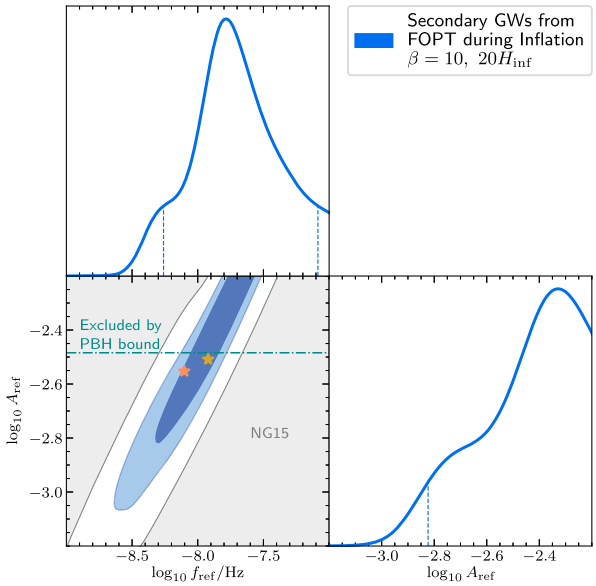

FIG. 5. The same as in Fig. 4 but for $\beta = 10, 20H_{\rm inf}$.

Summary and outlook. The main results of this work are shown in Fig. 2. As a benchmark, we compare them with data from the NANOGrav Collaboration. The observations from the other PTA collaborations are in broad agreement. The secondary GW signal considered in this work can

provide a comparable magnitude to account for the observed data and fit the spectral shape, particularly in the region $f < 3 \times 10^{-8}$ Hz. Hence, it is concluded that the GW production mechanism investigated in this paper offers a promising explanation for the observations made by PTA collaborations.

The observed signal in the higher frequency range $f > 3 \times 10^{-8}$ Hz seems to indicate an even higher amplitude. Further data and combining the data from all PTA collaborations can shed more light on this region. In the proposed scenario, it is possible, in principle, to consider slightly later phase transitions (smaller N_e) to shift the signal peak toward higher frequencies. Other parameters such as L, ϵ, and β can also be adjusted to achieve a higher amplitude. However, as already evident in Fig. 1, higher amplitudes of curvature perturbations will inevitably lead to copious production of primordial black holes and may be in tension with observations. This limitation applies to any mechanism of secondary GW production.

Significant PBH production is expected in the region with large curvature perturbations considered in this work, even if they have not been excluded yet. This could offer a correlated signal to verify the secondary GW production mechanism. A detailed investigation of this question is left for future work.

Acknowledgments. The work of H. A. is supported in part by the National Key R&D Program of China under Grants No. 2021YFC2203100 and No. 2017YFA0402204, the National Science Foundation of China under Grant No. 11975134, and the Tsinghua University Dushi Program No. 53120200422. The work of L.-T. W. is supported by the Department of Energy Grant No. DE-SC0013642.

[1] G. Agazie *et al.* (NANOGrav Collaboration), The NANOGrav 15 yr data set: Observations and timing of 68 millisecond pulsars, Astrophys. J. Lett. **951**, L9 (2023).
[2] J. Antoniadis *et al.*, The second data release from the European Pulsar Timing Array I. The dataset and timing analysis, Astron. Astrophys. **678**, A48 (2023).
[3] A. Zic *et al.*, The Parkes Pulsar Timing Array third data release, Pub. Astron. Soc. Aust. **40**, e049 (2023).
[4] H. Xu *et al.*, Searching for the nano-hertz stochastic gravitational wave background with the Chinese Pulsar Timing Array data release I, Res. Astron. Astrophys. **23**, 075024 (2023).
[5] G. Agazie *et al.* (NANOGrav Collaboration), The NANOGrav 15 yr data set: Evidence for a gravitational-wave background, Astrophys. J. Lett. **951**, L8 (2023).
[6] J. Antoniadis *et al.*, The second data release from the European Pulsar Timing Array III. Search for gravitational wave signals, Astron. Astrophys. **678**, A50 (2023).
[7] D. J. Reardon *et al.*, Search for an isotropic gravitational-wave background with the Parkes Pulsar Timing Array, Astrophys. J. Lett. **951**, L6 (2023).
[8] R. w. Hellings and G. s. Downs, Upper limits on the isotropic gravitational radiation background from Pulsar Timing Analysis, Astrophys. J. Lett. **265**, L39 (1983).
[9] G. Franciolini, D. Racco, and F. Rompineve, Footprints of the QCD crossover on cosmological gravitational waves at pulsar timing arrays, Phys. Rev. Lett. **132**, 081001 (2024).
[10] L. Zu, C. Zhang, Y.-Y. Li, Y.-C. Gu, Y.-L. S. Tsai, and Y.-Z. Fan, Mirror QCD phase transition as the origin of the nanohertz stochastic gravitational-wave background detected by the pulsar timing arrays, Sci. Bull. **69**, 741 (2024).
[11] C. Han, K.-P. Xie, J. M. Yang, and M. Zhang, Self-interacting dark matter implied by nano-Hertz gravitational waves, arXiv:2306.16966.
[12] K. Fujikura, S. Girmohanta, Y. Nakai, and M. Suzuki, NANOGrav signal from a dark conformal phase transition, Phys. Lett. B **846**, 138203 (2023).
[13] P. Athron, A. Fowlie, C.-T. Lu, L. Morris, L. Wu, Y. Wu, and Z. Xu, Can Supercooled phase transitions explain the gravitational wave background observed by pulsar timing arrays?, arXiv:2306.17239.
[14] A. Addazi, Y.-F. Cai, A. Marciano, and L. Visinelli, Have Pulsar Timing Array methods detected a cosmological phase transition?, Phys. Rev. D **109**, 015028 (2024).
[15] S. Jiang, A. Yang, J. Ma, and F. P. Huang, Implication of nano-Hertz stochastic gravitational wave on dynamical dark matter through a first-order phase transition, Classical Quantum Gravity **41**, 065009 (2024).
[16] K. Murai and W. Yin, A novel probe of supersymmetry in light of nanohertz gravitational waves, J. High Energy Phys. 10 (2023) 062.
[17] S.-P. Li and K.-P. Xie, A collider test of nano-Hertz gravitational waves from pulsar timing arrays, Phys. Rev. D **108**, 055018 (2023).
[18] Y. Xiao, J. M. Yang, and Y. Zhang, Implications of nanohertz gravitational waves on electroweak phase transition in the singlet dark matter model, Sci. Bull. **68**, 3158 (2023).
[19] T. Ghosh, A. Ghoshal, H.-K. Guo, F. Hajkarim, S. F. King, K. Sinha, X. Wang, and G. White, Did we hear the sound of the Universe boiling? Analysis using the full fluid velocity profiles and NANOGrav 15-year data, arXiv:2307.02259.
[20] K. T. Abe and Y. Tada, Translating nano-Hertz gravitational wave background into primordial perturbations taking account of the cosmological QCD phase transition, Phys. Rev. D **108**, L101304 (2023).
[21] X. K. Du, M. X. Huang, F. Wang, and Y. K. Zhang, Did the nHZ gravitational waves signatures observed by NANOGrav indicate multiple sector SUSY breaking?, arXiv:2307.02938.

[22] Y.-M. Wu, Z.-C. Chen, and Q.-G. Huang, Cosmological interpretation for the stochastic signal in pulsar timing arrays, Sci. China Phys. Mech. Astron. **67**, 240412 (2024).
[23] X.-F. Li, Probing the high temperature symmetry breaking with gravitational waves from domain walls, arXiv:2307.03163.
[24] J. S. Cruz, F. Niedermann, and M. S. Sloth, NANOGrav meets hot new early dark energy and the origin of neutrino mass, Phys. Lett. B **846**, 138202 (2023).
[25] P. Di Bari and M. H. Rahat, The split Majoron model confronts the NANOGrav signal, arXiv:2307.03184.
[26] Y. Gouttenoire, First-order phase transition interpretation of PTA signal produces solar-mass black holes, Phys. Rev. Lett. **131**, 171404 (2023).
[27] A. Salvio, Supercooling in radiative symmetry breaking: Theory extensions, gravitational wave detection and primordial black holes, J. Cosmol. Astropart. Phys. 12 (2023) 046.
[28] Z.-Q. Shen, G.-W. Yuan, Y.-Y. Wang, and Y.-Z. Wang, Dark matter spike surrounding supermassive black holes binary and the nanohertz stochastic gravitational wave background, arXiv:2306.17143.
[29] S.-Y. Guo, M. Khlopov, X. Liu, L. Wu, Y. Wu, and B. Zhu, Footprints of axion-like particle in pulsar timing array data and JWST observations, arXiv:2306.17022.
[30] G. Franciolini, A. Iovino, Jr., V. Vaskonen, and H. Veermae, The recent gravitational wave observation by pulsar timing arrays and primordial black holes: The importance of non-Gaussianities, Phys. Rev. Lett. **131**, 201401 (2023).
[31] J. Ellis, M. Fairbairn, G. Hütsi, J. Raidal, J. Urrutia, V. Vaskonen, and H. Veermäe, Gravitational waves from SMBH binaries in light of the NANOGrav 15-year data, Phys. Rev. D **109**, L021302 (2024).
[32] T. Broadhurst, C. Chen, T. Liu, and K.-F. Zheng, Binary supermassive black holes orbiting dark matter solitons: From the dual AGN in UGC4211 to nanohertz gravitational waves, arXiv:2306.17821.
[33] H.-L. Huang, Y. Cai, J.-Q. Jiang, J. Zhang, and Y.-S. Piao, Supermassive primordial black holes in multiverse: For nano-Hertz gravitational wave and high-redshift JWST galaxies, arXiv:2306.17577.
[34] Y.-C. Bi, Y.-M. Wu, Z.-C. Chen, and Q.-G. Huang, Implications for the supermassive black hole binaries from the NANOGrav 15-year data set, Sci. China Phys. Mech. Astron. **66**, 120402 (2023).
[35] C. Zhang, N. Dai, Q. Gao, Y. Gong, T. Jiang, and X. Lu, Detecting new fundamental fields with pulsar timing arrays, Phys. Rev. D **108**, 104069 (2023).
[36] Y. Gouttenoire, S. Trifinopoulos, G. Valogiannis, and M. Vanvlasselaer, Scrutinizing the primordial black holes interpretation of PTA gravitational waves and JWST early galaxies, arXiv:2307.01457.
[37] H. An and C. Yang, Gravitational waves produced by domain walls during inflation, arXiv:2304.02361.
[38] Z. Wang, L. Lei, H. Jiao, L. Feng, and Y.-Z. Fan, The nanohertz stochastic gravitational-wave background from cosmic string Loops and the abundant high redshift massive galaxies, Sci. China Phys. Mech. Astron. **66**, 120403 (2023).
[39] J. Ellis, M. Lewicki, C. Lin, and V. Vaskonen, Cosmic superstrings revisited in light of NANOGrav 15-year data, Phys. Rev. D **108**, 103511 (2023).
[40] N. Kitajima, J. Lee, K. Murai, F. Takahashi, and W. Yin, Nanohertz gravitational waves from axion domain walls coupled to QCD, Phys. Lett. B **851**, 138586 (2024).
[41] Y. Bai, T.-K. Chen, and M. Korwar, QCD-collapsed domain walls: QCD phase transition and gravitational wave spectroscopy, J. High Energy Phys. 12 (2023) 194.
[42] N. Kitajima and K. Nakayama, Nanohertz gravitational waves from cosmic strings and dark photon dark matter, Phys. Lett. B **846**, 138213 (2023).
[43] G. Lazarides, R. Maji, and Q. Shafi, Superheavy quasi-stable strings and walls bounded by strings in the light of NANOGrav 15 year data, Phys. Rev. D **108**, 095041 (2023).
[44] P. F. Depta, K. Schmidt-Hoberg, and C. Tasillo, Do pulsar timing arrays observe merging primordial black holes?, arXiv:2306.17836.
[45] L. Bian, S. Ge, J. Shu, B. Wang, X.-Y. Yang, and J. Zong, Gravitational wave sources for pulsar timing arrays, Phys. Rev. D **109**, L101301 (2024).
[46] B. Barman, D. Borah, S. Jyoti Das, and I. Saha, Scale of Dirac leptogenesis and left-right symmetry in the light of recent PTA results, J. Cosmol. Astropart. Phys. 10 (2023) 053.
[47] S. Antusch, K. Hinze, S. Saad, and J. Steiner, Singling out SO(10) GUT models using recent PTA results, Phys. Rev. D **108**, 095053 (2023).
[48] E. Babichev, D. Gorbunov, S. Ramazanov, R. Samanta, and A. Vikman, NANOGrav spectral index $\gamma = 3$ from melting domain walls, Phys. Rev. D **108**, 123529 (2023).
[49] W. Buchmuller, V. Domcke, and K. Schmitz, Metastable cosmic strings, J. Cosmol. Astropart. Phys. 11 (2023) 020.
[50] M. Yamada and K. Yonekura, Dark baryon from pure Yang-Mills theory and its GW signature from cosmic strings, J. High Energy Phys. 09 (2023) 197.
[51] S. Ge, Stochastic gravitational wave background: Birth from axionic string-wall death, arXiv:2307.08185.
[52] Z. Zhang, C. Cai, Y.-H. Su, S. Wang, Z.-H. Yu, and H.-H. Zhang, Nano-Hertz gravitational waves from collapsing domain walls associated with freeze-in dark matter in light of pulsar timing array observations, Phys. Rev. D **108**, 095037 (2023).
[53] S. Vagnozzi, Inflationary interpretation of the stochastic gravitational wave background signal detected by pulsar timing array experiments, J. High Energy Astrophys. **39**, 81 (2023).
[54] V. K. Oikonomou, Flat energy spectrum of primordial gravitational waves vs peaks and the NANOGrav 2023 observation, Phys. Rev. D **108**, 043516 (2023).
[55] S. Datta, Inflationary gravitational waves, pulsar timing data and low-scale-leptogenesis, Phys. Rev. D **108**, L091706 (2023).
[56] D. Borah, S. Jyoti Das, and R. Samanta, Inflationary origin of gravitational waves with miracle-less WIMP dark matter in the light of recent PTA results, J. Cosmol. Astropart. Phys. 03 (2024) 031.
[57] S. Wang, Z.-C. Zhao, J.-P. Li, and Q.-H. Zhu, Exploring the implications of 2023 pulsar timing array datasets for scalar-induced gravitational waves and primordial black holes, Phys. Rev. Res. **6**, L012060 (2024).
[58] B.-M. Gu, F.-W. Shu, and K. Yang, Inflation with shallow dip and primordial black holes, arXiv:2307.00510.

[59] D. Chowdhury, G. Tasinato, and I. Zavala, Dark energy, D-branes, and Pulsar Timing Arrays, J. Cosmol. Astropart. Phys. 11 (2023) 090.
[60] X. Niu and M. H. Rahat, NANOGrav signal from axion inflation, Phys. Rev. D **108**, 115023 (2023).
[61] R. Ebadi, S. Kumar, A. McCune, H. Tai, and L.-T. Wang, Gravitational waves from stochastic scalar fluctuations, Phys. Rev. D **109**, 083519 (2024).
[62] Z. Yi, Q. Gao, Y. Gong, Y. Wang, and F. Zhang, The waveform of the scalar induced gravitational waves in light of pulsar timing array data, Sci. China Phys. Mech. Astron. **66**, 120404 (2023).
[63] D. G. Figueroa, M. Pieroni, A. Ricciardone, and P. Simakachorn, Cosmological background interpretation of pulsar timing array data, Phys. Rev. Lett. **132**, 171002 (2024).
[64] C. Unal, A. Papageorgiou, and I. Obata, Axion-gauge dynamics during inflation as the origin of pulsar timing array signals and primordial black holes, arXiv:2307.02322.
[65] H. Firouzjahi and A. Talebian, Induced gravitational waves from ultra slow-roll inflation and pulsar timing arrays observations, J. Cosmol. Astropart. Phys. 10 (2023) 032.
[66] Q.-H. Zhu, Z.-C. Zhao, and S. Wang, Joint implications of BBN, CMB, and PTA datasets for scalar-induced gravitational waves of second and third orders, Phys. Rev. Res. **6**, 013207 (2024).
[67] S. Choudhury, Single field inflation in the light of NANOGrav 15-year Data: Quintessential interpretation of blue tilted tensor spectrum through non-Bunch Davies initial condition, Eur. Phys. J. C **84**, 278 (2024).
[68] Z.-Q. You, Z. Yi, and Y. Wu, Constraints on primordial curvature power spectrum with pulsar timing arrays, J. Cosmol. Astropart. Phys. 11 (2023) 065.
[69] S. A. Hosseini Mansoori, F. Felegray, A. Talebian, and M. Sami, PBHs and GWs from $\mathbb{T}^2$-inflation and NANOGrav 15-year data, J. Cosmol. Astropart. Phys. 08 (2023) 067.
[70] K. Cheung, C. J. Ouseph, and P.-Y. Tseng, NANOGrav signal and PBH from the modified Higgs inflation, arXiv:2307.08046.
[71] S. Basilakos, D. V. Nanopoulos, T. Papanikolaou, E. N. Saridakis, and C. Tzerefos, Signatures of superstring theory in NANOGrav, Phys. Lett. B **850**, 138507 (2024).
[72] J.-H. Jin, Z.-C. Chen, Z. Yi, Z.-Q. You, L. Liu, and Y. Wu, Confronting sound speed resonance with pulsar timing arrays, J. Cosmol. Astropart. Phys. 09 (2023) 016.
[73] S. Balaji, G. Domènech, and G. Franciolini, Scalar-induced gravitational wave interpretation of PTA data: The role of scalar fluctuation propagation speed, J. Cosmol. Astropart. Phys. 10 (2023) 041.
[74] M. Bousder, A. Riadsolh, A. E. Fatimy, M. E. Belkacemi, and H. Ez-Zahraouy, Implications of the NANOGrav results for primordial black holes and Hubble tension, arXiv:2307.10940.
[75] H.-H. Li, G. Ye, and Y.-S. Piao, Is the NANOGrav signal a hint of dS decay during inflation?, Phys. Lett. B **816**, 136211 (2021).
[76] E. Madge, E. Morgante, C. Puchades-Ibáñez, N. Ramberg, W. Ratzinger, S. Schenk, and P. Schwaller, Primordial gravitational waves in the nano-Hertz regime and PTA data—Towards solving the GW inverse problem, J. High Energy Phys. 10 (2023) 171.
[77] Y. Li, C. Zhang, Z. Wang, M. Cui, Y.-L. S. Tsai, Q. Yuan, and Y.-Z. Fan, Primordial magnetic field as a common solution of nanohertz gravitational waves and Hubble tension, Phys. Rev. D **109**, 043538 (2024).
[78] J. Yang, N. Xie, and F. P. Huang, Nano-Hertz stochastic gravitational wave background as hints of ultralight axion particles, arXiv:2306.17113.
[79] L. A. Anchordoqui, I. Antoniadis, and D. Lust, Fuzzy dark matter, the dark dimension, and the pulsar timing array signal, Eur. Phys. J. C **84**, 273 (2024).
[80] R. A. Konoplya and A. Zhidenko, Asymptotic tails of massive gravitons in light of pulsar timing array observations, Phys. Lett. B **853**, 138685 (2024).
[81] M. Geller, S. Ghosh, S. Lu, and Y. Tsai, Challenges in interpreting the NANOGrav 15-year data set as early universe gravitational waves produced by ALP induced instability, Phys. Rev. D **109**, 063537 (2024).
[82] G. B. Gelmini and J. Hyman, Catastrogenesis with unstable ALPs as the origin of the NANOGrav 15 yr gravitational wave signal, Phys. Lett. B **848**, 138356 (2024).
[83] H. Jiang, T. Liu, S. Sun, and Y. Wang, Echoes of inflationary first-order phase transitions in the CMB, Phys. Lett. B **765**, 339 (2017).
[84] H. An, K.-F. Lyu, L.-T. Wang, and S. Zhou, A unique gravitational wave signal from phase transition during inflation*, Chin. Phys. C **46**, 101001 (2022).
[85] H. An, K.-F. Lyu, L.-T. Wang, and S. Zhou, Gravitational waves from an inflation triggered first-order phase transition, J. High Energy Phys. 06 (2022) 050.
[86] J. Barir, M. Geller, C. Sun, and T. Volansky, Gravitational waves from incomplete inflationary phase transitions, Phys. Rev. D **108**, 115016 (2023).
[87] D. Baumann, P. J. Steinhardt, K. Takahashi, and K. Ichiki, Gravitational wave spectrum induced by primordial scalar perturbations, Phys. Rev. D **76**, 084019 (2007).
[88] K. Kohri and T. Terada, Semianalytic calculation of gravitational wave spectrum nonlinearly induced from primordial curvature perturbations, Phys. Rev. D **97**, 123532 (2018).
[89] P. Adshead, K. D. Lozanov, and Z. J. Weiner, Non-Gaussianity and the induced gravitational wave background, J. Cosmol. Astropart. Phys. 10 (2021) 080.
[90] See Supplemental Material at http://link.aps.org/supplemental/10.1103/PhysRevD.109.L121304 for the detailed phase transition model, the lattice simulation method employed in our numerical simulation, and an analysis of the form factor. We also provide a thorough explanation of the calculation of the Bayes factor.
[91] C. T. Byrnes, P. S. Cole, and S. P. Patil, Steepest growth of the power spectrum and primordial black holes, J. Cosmol. Astropart. Phys. 06 (2019) 028.
[92] A. Afzal *et al.* (NANOGrav Collaboration), The NANOGrav 15 yr data set: Search for signals from new physics, Astrophys. J. Lett. **951**, L11 (2023).
[93] A. Mitridate, D. Wright, R. von Eckardstein, T. Schröder, J. Nay, K. Olum, K. Schmitz, and T. Trickle, PTArcade, arXiv:2306.16377.